PHYSICAL REVIEW B VOLUME 34, NUMBER 4 15 AUGUST 1986

Optical properties of pure and ultraheavily doped germanium: Theory and experiment

L. Viña* and M. Cardona
Max-Planck-Institut für Festkörperforschung, Heisenbergstrasse 1, D-7000 Stuttgart 80, Federal Republic of Germany
(Received 30 December 1985)

We have measured by spectroellipsometry the dielectric function ϵ of pure and ultraheavily doped germanium from the near-infrared ($\hbar\omega \simeq 1.6$ eV) to the near-ultraviolet ($\hbar\omega \simeq 5.6$ eV) regions. The dependence of the E_1, $E_1+\Delta_1$, E_0', and E_2 critical energies on impurity concentration was obtained. A red shift of the different critical-point energies, together with an increase of the lifetime broadening, has been observed. Amplitudes and phase angles for the corresponding critical points were also obtained. The results are compared with full band-structure calculations of the effect of the impurities on the band structure of germanium.

I. INTRODUCTION

Considerable attention has been devoted in the past years to the effect of heavy doping on the electronic properties of semiconductors.[1-3] Besides the technological importance of obtaining high doping levels, e.g., for the tailoring of device properties, it is of basic interest to study the energy spectra of disordered materials and to compare the experimental results with theoretical predictions of the change and of band structure with impurity concentration. At moderate low doping levels localized impurity states develop close to the band edges. With increasing dopant concentration the localized states overlap, producing an impurity band. This band is separated from the host conduction (valence) band (for the case of donors, acceptors, respectively) by the so-called Mott gap. At still higher impurity concentrations, the impurity and the host band become mixed to build a new continuum, so that there is no longer a clear distinction between band and impurity states. In this way the degenerate semiconductor resembles a metal.

The effects of doping on the fundamental band edges have been studied with electrical transport experiments[4] as well as with optical techniques such as absorption,[5,6] electroreflectance[7] (ER), and photoluminescence.[8] Besides the formation of band tails because of the random potential, a shift of the band edges results, due to two competing phenomena: a blue shift (Moss-Burstein shift[9]) due to the filling of the valence (conduction) band by holes (electrons), and a shrinkage by many-body effects.

The higher edges, above the fundamental ones, have been less studied. Only optical measurements, such as reflectivity,[10-13] ER,[14-17] photoluminescence,[18] and ellipsometry[19] have been carried out. Recently, resonant Raman scattering by phonons in heavily doped n-type Ge for the region of the E_1 and $E_1+\Delta_1$ has been studied.[20]

The spectroellipsometry technique has been proven as a reliable tool to measure the effects of heavy doping on the band structure of semiconductors.[19,21-23] This technique measures the complex pseudo-dielectric-function versus photon energy (the term "pseudo" will be used in the rest of the paper because of small effects of uncharacterized surface layers). The structures present in the spectra are believed to be related to interband transitions at different points of the Brillouin zone (BZ). The usually broad features can be enhanced by means of numerical derivative techniques. A line-shape analysis of these data yields not only an accurate determination of the energy threshold (E), but also detailed information about the electronic interband transition, such as lifetime broadening (Γ), oscillator strength (A), and many-body effects, described by the phase angle ϕ.

In this paper we report on the optical properties of pure and ultraheavily doped germanium measured at room temperature in the region from near infrared (1.8 eV) to the near ultraviolet (5.6 eV). Bulk-doped and ion-implanted, laser-annealed (IILA) germanium was used to prepare samples, with impurity concentration ranging from $N \simeq 10^{13}$ cm^{-3} to $N \simeq 2\times10^{21}$ cm^{-3}. The use of IILA samples provides doping levels one order of magnitude higher then the bulk thermal solubility limit[24] ($N_e \simeq 4\times10^{19}$ cm^{-3}), and therefore allows us to extend the range of electrically active, impurity concentration of our previous work.[19]

We have carefully studied the higher interband transitions labeled E_1 ($\simeq 2.1$ eV), $E_1+\Delta_1$ ($\simeq 2.3$ eV), E_0' ($\simeq 3.1$ eV), and E_2 ($\simeq 4.4$ eV). Two-dimensional (2D) line shapes were used to analyze the line shape of all these critical points (CP). We find that the main effect of the dopants is to broaden the CP and to shift them to lower energies. Another effect we find is a systematic decrease of the excitonic phase angle ϕ with increasing impurity concentration, as well as a decrease of the oscillator strength of the E_1 CP in n-type material, in agreement with the decrease in intensity found for the resonant Raman scattering,[20] and attributed to the presence of free electrons at the L minima of the conduction band.

We have performed perturbation calculations of the changes in the band structure of Ge due to substitutional impurities,[23,25] including terms of first and second order in the impurity potential. We have extended the results of our previous work[23] (in the following referred to as VC) and calculated the effects of acceptors as well as donors on the critical points of Ge; both kinds of impurities yield similar shifts and broadenings of the different singularities with an N^α dependence. This dependence is in

 ©1986 The American Physical Society

TABLE I. Samples used for the ellipsometric measurements shown in Figs. 1 and 2. ? indicates direction was unknown.

		Doping concentration (cm^{-3})	Implantation dose (cm^{-2})	Implantation energy (keV)	Carrier concentration[a] (cm^{-3})
Undoped Ge	[110]				$<10^{13}$
n-type Ge(As-V)	[111]	2.7×10^{19}			2.7×10^{19}
p-type Ge(Ga-V)	[110]	7.8×10^{19}			7.8×10^{19}
n-type Ge(P-VI)	[100]	9.5×10^{20}	2×10^{16}	190	1.2×10^{20}
p-type Ge(In-I)	?	2×10^{21}	2×10^{16}	350	1.6×10^{21}

[a]Estimated as in Ref. 44.

reasonable agreement with the experimental results.

The outline of this paper is as follows. Section II gives the experimental details. The results are presented in Sec. III. Section IV deals with the method of calculation, and finally the experimental results are discussed in the light of the theoretical calculations in Sec. V.

II. EXPERIMENT

Pure and n- and p-type bulk-doped Ge crystals with doping concentrations from 6×10^{17} to 8×10^{19} cm^{-3} were used to prepare samples. A standard polishing procedure[23] was used to obtain mirrorlike surfaces. We also used IILA (Ref. 26) crystals with ion concentrations ranging from 2×10^{19} to 2×10^{21} cm^{-3}. The range of implantation doses was $(0.2-6)\times10^{16}$ cm^{-2} for n-type material and $(1-6)\times10^{16}$ cm^{-2} for p-type material at 65–350 keV. The crystals were annealed with a XeCl excimer laser at 308 nm. The annealed surface was obtained by multiple overlapping laser spots as described in Ref. 27. The typical laser energy per shot was 0.8 J/cm^2.

We present here the complete spectra of ϵ_1 and ϵ_2 and their second derivatives for 5 of the 26 samples measured. Only the critical-point parameters are given for the rest of the samples. The characteristics of these samples are summarized in Table I. The first sample, taken as reference and labeled as undoped or pure Ge, has a very low electron concentration at 77 K ($n<10^{13}$ cm^{-3}). Two samples are bulk doped with arsenic [n-type Ge (As-V)] and with gallium [p-type Ge (Ga-V)] with carrier concentrations of $n=2.7\times10^{19}$ cm^{-3} and $p=7.8\times10^{19}$ cm^{-3}. The last two samples are IILA crystals implanted with phosphorus [n-type Ge (P-VI); $n=1.2\times10^{20}$ cm^{-3}] and indium [p-type Ge (In-I); $p=2\times10^{21}$ cm^{-3}].

An automatic ellipsometer described elsewhere[23] was used to measure the pseudo-dielectric-function spectra $\epsilon(\omega)=\epsilon_1(\omega)+i\epsilon_2(\omega)$ at room temperature between 1.8 and 5.6 eV. The samples were mounted and optically aligned in a windowless cell in flowing N_2 to minimize surface contamination. The chemical treatment of the samples was described previously in VC.

III. RESULTS

Pseudo-dielectric-functions were calculated from the complex Fresnel's reflectance ratios, with the use of the measured ellipsometric angles (Ψ,Δ) and taking into account the optical activity of the Rochon prisms.[28] The spectra for the five selected samples are shown in Figs. 1(a)–1(d), where the dotted lines represent the pseudo-dielectric-function of undoped Ge. The effect of the impurities is clearly seen in these figures: There is an increasing lifetime broadening and red shift in the E_1 (2.1 eV), $E_1+\Delta_1$ (2.3 eV), E_0' (3.1 eV), and E_2 (4.4 eV). For the spectra of Figs. 1(a) and 1(b) we have assumed that the ellipsometric data correspond to a simple air-bulk-Ge interface and a two-phase model[29] was used. For the IILA samples an oxide film is still present,[30] whose thickness is estimated to be about 25 Å, as Ge and Si react similarly to the etchants.[23] In this case we used a three-phase model (air-GeO_2-Ge) for the treatment of the data. The index of refraction of the GeO_2 overlayer was taken from the literature.[31] The equations were solved to obtain $\epsilon(\omega)$ using the two-dimensional Newton method.[32] As a check of our spectra we have calculated the following sum rules:[33]

$$N_{\text{eff}}=\frac{2m}{4\pi^2e^2N_{\text{atom}}}\int_{\omega_m}^{\omega_M}\omega\epsilon_2(\omega)d\omega\ , \tag{1a}$$

$$\tilde{\epsilon}_1(\omega_0)=1+\frac{2}{\pi}\text{P}\int_{\omega_m}^{\omega_M}\frac{\omega\epsilon_2(\omega)}{\omega^2-\omega_0^2}d\omega\ , \tag{1b}$$

where N_{atom} is the atomic density, m and e are the mass and charge of the electron, respectively, and P means the Cauchy principal value of the integral. For $\omega_m\to0$ and $\omega_M\to\infty$, Eq. (1a) would yield N_{eff} slightly larger than 4 and $\tilde{\epsilon}_1(\omega_0)=\epsilon_1(\omega_0)$. We take $\omega_m=1.8$ eV, $\omega_M=5.6$ eV, and calculate the integrals for $\omega_0=2.01$ eV. The values obtained for N_{eff} and $\tilde{\epsilon}_1(\omega)$ are listed in Table II. N_{eff} for the pure sample is 2.47, in good agreement with the determination of Phillipp and Ehrenreich.[34] N_{eff} decreases with increasing doping concentration, similarly to the case of Si (Ref. 23). The sum rule for $\tilde{\epsilon}_1$ [Eq. (1b)] converges much more rapidly than that for N_{eff}: for the undoped and bulk-doped samples, $\epsilon_1(2.01)-\tilde{\epsilon}_1(2.01)$ is smaller than 1. This value increases to 2.2 for the IILA samples, indicating that we are really measuring a pseudo-dielectric-function containing small effects of an uncharacterized overlayer.

Second-derivative spectra ($d^2\epsilon/d\omega^2$) of the complex pseudo-dielectric-function with respect to the photon energy calculated numerically from our ellipsometric data were used to obtain the shifts and broadenings of the CP. The results for ($d^2\epsilon_2/d\omega^2$) are shown in Fig. 2 for the five samples. The solid lines correspond to the numerical derivatives of the spectra of Fig. 1; the dashed lines are the best fit to the experimental ones.

The second-derivative spectra show a red shift of the

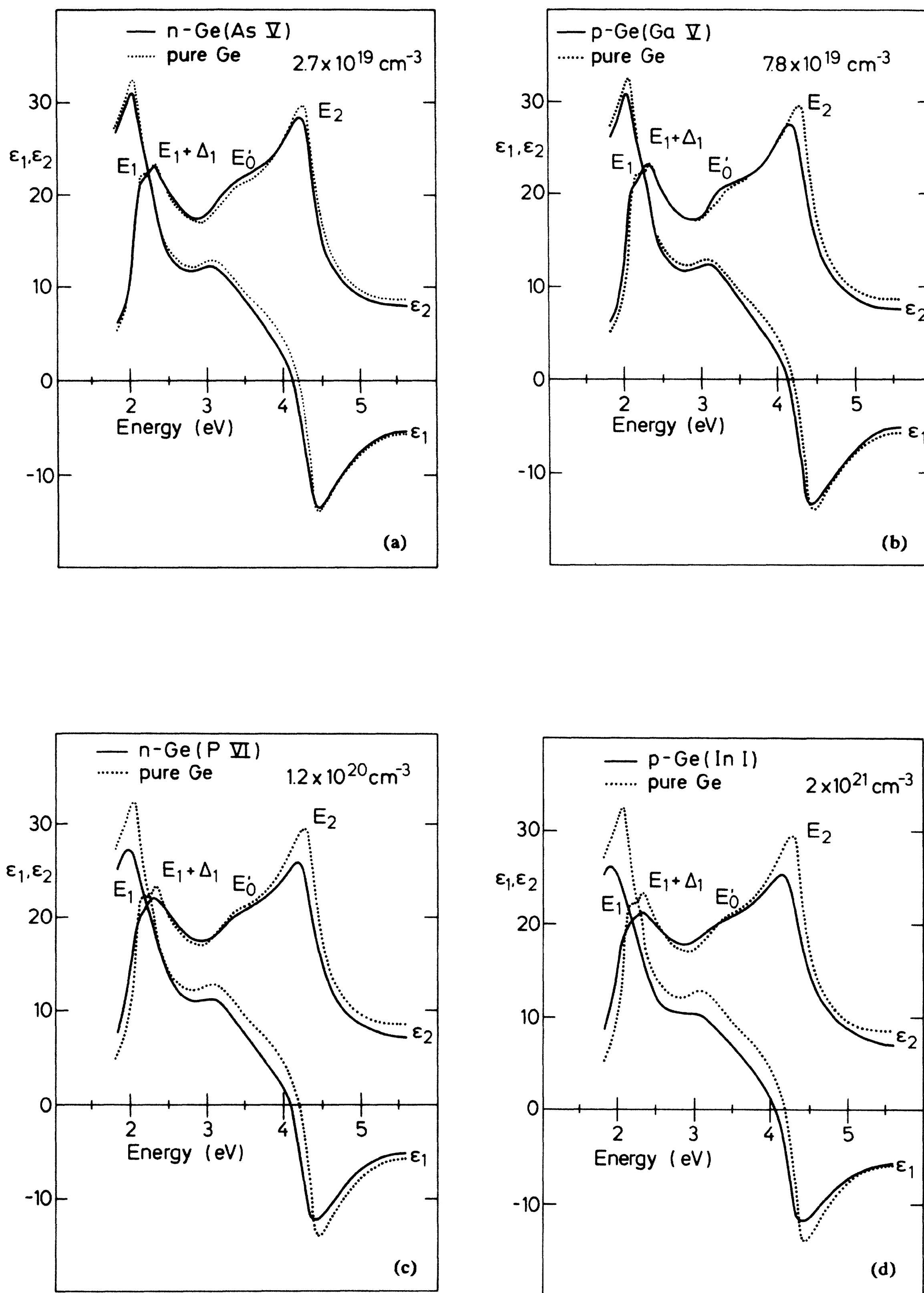

FIG. 1. Solid curves: real (ϵ_1) and imaginary (ϵ_2) parts of the pseudo-dielectric-function of (a) bulk Ge, arsenic doped with $n = 2.7\times10^{19}$ cm^{-3}; (b) bulk Ge, gallium doped ($p = 7.8\times10^{19}$ cm^{-3}); (c) phosphorus-implanted, laser-annealed Ge ($n = 1.2\times10^{20}$ cm^{-3}); (d) indium-implanted, laser-annealed Ge ($p = 2\times10^{21}$ cm^{-3}). For comparison the pseudo-dielectric-function for pure Ge ($n < 10^{13}$ cm^{-3}) is also shown as dotted lines in (a)—(d).

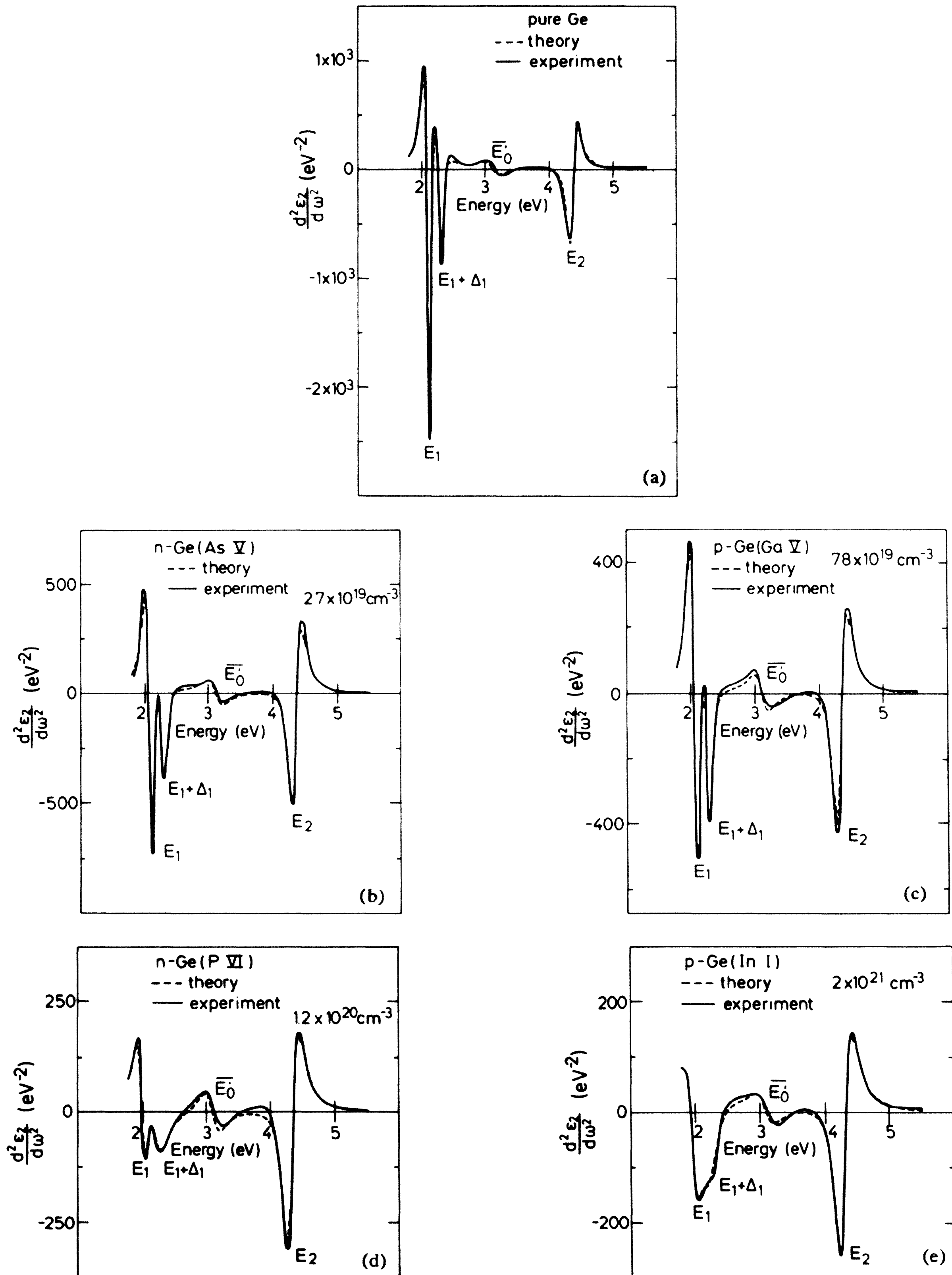

FIG. 2. Solid curves: second derivatives with respect to the photon energy of the imaginary part of the pseudo-dielectric-function ($d^2\epsilon_2/d\omega^2$) of the spectra shown in Fig. 1. (a) undoped Ge; (b) n-type Ge (As-V); (c) p-type Ge (Ga-V); (d) n-type Ge (P-VI); (e) p-type Ge (In-I) (the notation for the samples is explained in Table I). Dashed curves: best fit of the E_1, $E_1+\Delta_1$, E_0', and E_2 singularities. A mixture of a two-dimensional minimum and saddle point was used for E_1 and $E_1+\Delta_1$, a two-dimensional minimum for E_0', and a mixture of a saddle point with a maximum was assumed for E_2. Note the changes in the vertical scale with increasing doping concentration.

TABLE II. Effective number of electrons n_{eff}, real part of pseudo-dielectric-function obtained through Kramers-Kronig transformation $\tilde{\epsilon}_1$, measured real part of pseudo-dielectric-function ϵ_1, and difference $\epsilon_1-\tilde{\epsilon}_1$, for the five samples of Figs. 1 and 2.

	Pure Ge	n-type Ge (As-V)	p-type Ge (Ga-V)	n-type Ge (P-VI)	p-type Ge (In-I)
n_{eff}	2.47	2.34	2.15	2.1	2.1
$\tilde{\epsilon}_1$ (2.01 eV)	30.6	29.6	29.7	25.4	23.7
ϵ_1 (2.01 eV)	31.7	30.4	30.4	27.6	25.4
$\epsilon_1-\tilde{\epsilon}_1$	1.1	0.8	0.7	2.2	1.7

energy positions of the CP from the pure to the highest doped sample, with a corresponding increase in their Lorentzian width Γ. These spectra were fitted assuming two-dimensional singularities for all the critical points.[35,36] Excitonic effects were also taken into account in a standard way by allowing a mixture of two critical points.[35–37] Both the real and the imaginary parts of $(d^2\epsilon/d\omega^2)$ were simultaneously fitted.

The mixture of contiguous two-dimensional critical points can be expressed by[35–37]

$$\epsilon=A-\ln(\omega_0-\omega-i\Gamma)e^{i\phi}\ , \tag{2}$$

where the angle ϕ represents the amount of mixture. In Fig. 3 we plot the values of $\tan\phi$ of the E_1 singularity obtained from our fits versus impurity concentration N_i. A mixture of a 2D minimum with a 2D saddle point corresponds to the values of ϕ $(0\leq\phi\leq\pi/2)$ obtained from the fit of the E_1 and $E_1+\Delta_1$ line shapes. These line shapes were simultaneously fitted assuming a constant spin-orbit splitting of 187 meV (Ref. 36). Similarly, a mixture of a 2D saddle point with a 2D maximum $(\pi/2\leq\phi\leq\pi)$ was found to fit best the E_2 CP. For the E_0' critical point a 2D minimum was used. We want to comment that the choice of a 2D—instead of a 3D—critical point for the E_0' structure is probably forced by the fact that at room temperature it was not possible to resolve the spin-split

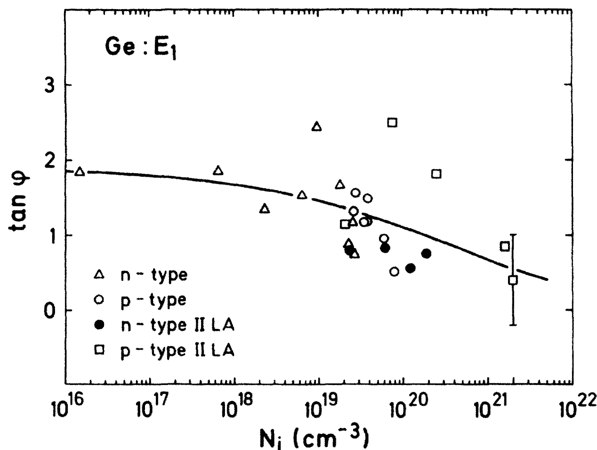

FIG. 3. Dependence on doping concentration of the excitonic parameter $\tan\phi$ defined in Eq. (2) for the E_1 critical point of Ge. Triangles, n-type bulk Ge; open circles, p-type bulk Ge; solid circles, n-type IILA Ge; squares, p-type IILA Ge. Solid line, best fit obtained using Eq. (30) of Ref. 23.

components of this singularity. The critical energies obtained from such analysis should thus represent a mean value of the E_0' and the $E_0'+\Delta_0'$ and therefore this structure will be labeled in the figures as $\bar{E}_0'$. The E_1 and $E_1+\Delta_1$ structures broaden considerably more than the E_0' and E_2 CP and their amplitudes decrease with increasing dopant concentration. Other features present in the spectra of Figs. 2(a)—2(e) is the decrease in the amplitude of the E_1 structure with respect to that of the $E_1+\Delta_1$ with increasing doping. In pure Ge E_1 is much stronger than the $E_1+\Delta_1$ CP [Fig. 2(a)], while for the sample P VI [Fig. 2(d)] both amplitudes are nearly the same.

The red shifts of the critical points E_1, E_0', and E_2 obtained from measurements of many bulk and implanted samples are shown in Figs. 4(a)—4(c) plotted versus carrier concentration in a double-logarithmic scale. In the case of the E_0' CP [Fig. 4(a)] only data points corresponding to red shifts are shown: Some samples of relatively small N_i gave blue shifts which were nevertheless negligible within error. The shifts found for $E_1+\Delta_1$ are the same as those of the E_1 CP because of our fitting procedure. The effect of doping becomes clearly noticeable for concentrations above 10^{19} cm^{-3}, as in the case of Si (Ref. 23). The energies and Lorentzian broadenings of the CP of pure Ge are listed in Table III; the red shifts ΔE and the enhancement of the Lorentzian broadening parameters $\Delta\Gamma$ are always referred to the values of pure Ge. The use of IILA samples allows us to obtain doping concentrations far above the solubility limit,[38] and thus increases the range obtained with bulk samples.[19] The results from the IILA samples join smoothly with those of the bulk samples, as can be seen in Figs. 4(a)—4(c). The dashed lines in these figures represent the best fit to a N_i^{α} law. We have not made separate fits for the n- and p-type samples since the observed shifts for a given doping concentration are independent of type within the experimental accuracy.

The increase in the Lorentzian broadening parameter Γ with respect to the undoped sample obtained from our line-shape analysis of the E_1, $E_1+\Delta_1$, and E_2 CP is shown in Figs. 5(a)—5(b). Due to the lack of spin-orbit coupling on our theoretical calculation of the effect of the impurities on the band structure of Ge, we have chosen to represent the mean value of the increase of Γ for the E_1 and $E_1+\Delta_1$ structures $[\Delta(\langle\Gamma_{E_1}+\Gamma_{E_1+\Delta_1}\rangle_{\mathrm{av}})]$. We do not show the broadening parameter for the E_0' structure, because the 2D line shape assumed, affected as mentioned above by unresolved spin-orbit splitting, is not expected to yield the actual value of the lifetime broadening of this CP.

TABLE III. Energies and broadening parameters of the critical points of pure Ge at room temperature. The values in parentheses show the 95% fit reliability.

E_1 (eV)	$E_1+\Delta_1$ (eV)	E'_0 (eV)	E_2 (eV)	$\Gamma(E_1)$ (meV)	$\Gamma(E_1+\Delta_1)$ (meV)	$\Gamma(E_2)$ (meV)
2.111(3)	2.298(3)	3.11(2)	4.368(4)	58(5)	73(10)	109(4)

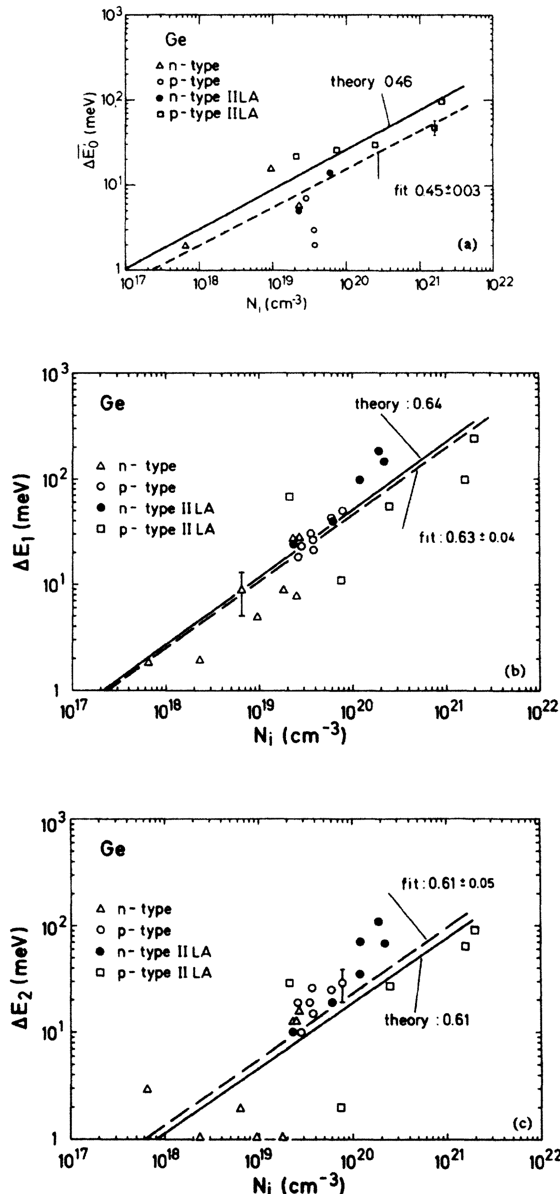

FIG. 4. Dependence on doping concentration of critical-point energies of Ge: (a) red shifts ($\Delta E'_0$) for the E'_0 singularity; (b) red shifts (ΔE_1) for the E_1 singularity; (c) red shift (ΔE_2) for the E_2 singularity. The symbols have the same meaning as in Fig. 3. Dashed lines, best fits to a N_I^{α} law, yielding $\alpha=0.45\pm0.03$ for E'_0, $\alpha=0.63\pm0.04$ for E_1, and $\alpha=0.61\pm0.05$ for E_2. Solid line, result of second-order perturbation-theory calculation. The shifts are measured with respect to the undoped sample.

IV. THEORY

Sections IV A and IV B of VC, discussing the general approach of the calculation and the first-order perturbation terms for Si, remain valid for Ge and will not be reproduced here. The pseudopotential form factors used for the calculations of the first-order perturbation terms, obtained in the same way as in VC, are listed in Table IV. In Table V we show the results of the calculation of the first-order perturbation terms obtained in the "virtual crystal approximation" (VCA), for the $E_0(\Gamma_{25'}\rightarrow\Gamma_{2'})$, $E'_0(\Gamma_{25'}\rightarrow\Gamma_{15})$, $E_{\rm ind}(\Gamma_{25'}\rightarrow X_1)$, $E_{\rm ind}(\Gamma_{25'}\rightarrow L_1)$, $E_1(\Lambda_{3'}\rightarrow\Lambda_3)$, $E'_1(\Lambda_{3'}\rightarrow\Lambda_3)$, and E_2 gaps of Ge. For the E_2 gap we took the point $\mathbf{k}=[(2\pi/a_0)](0.75,0.25,0.25)$ as representative of this transition.[39]

For the E_1 transitions we have calculated the shifts for several points along the Λ direction $\mathbf{k}=[(\pi y/a_0)](1,1,1)$ and averaged them for $\frac{1}{4}\leq y\leq 1$. At E'_1 we used the same procedure while averaging for $\frac{1}{2}\leq y\leq 1$. These regions of y should contribute mostly to the observed structure (parallel valence and conduction bands[39]).

In Table V we also show the linear coefficients of the shifts of Ge gaps with doping, calculated as described in Sec. IV B of Ref. 23. Here, and in the rest of the article, positive shifts mean *red* shifts with increasing doping concentration. The shifts in Table V are usually about an order of magnitude smaller than the second-order shifts, to be discussed later; the only exceptions are found, as in the case of Si, in the case of N and B doping. We must, however, bear in mind that in these cases the pseudopotentials are not well known. In most cases gaps which exhibit blue shifts for donors show red shifts for acceptors.

The terms in first-order perturbation yield only a real self-energy contribution (energy shift) and they do not affect the lifetime of the electronic states. The next terms in the perturbation series are represented schematically in Fig. 6 [cf. Eq. (15) in Ref. 23]: These terms represent second-order processes via a virtual intermediate state (scattering of an electron initially in the one-particle state $|\mathbf{k},n\rangle$ into another one-particle state $|\mathbf{k}+\mathbf{q},m\rangle$ and back to $|\mathbf{k},n\rangle$). Two kinds of processes can be distinguished: intraband scattering, in which the virtual intermediate state is in the same band as the initial state ($m=n$), and interband scattering ($n\neq m$). Generally, the energy denominators involved in these second-order terms are larger for the interband than for the intraband scattering, thus the latter processes usually dominate.

In Ref. 23 we presented calculations of the second-order terms for the case of acceptors in Si. The case of donors differs because of the details of the corresponding band

TABLE IV. Pseudopotential form factors V_3, V_8, and V_{11} (in Ry) used for the calculations of the first-order effect of impurities on the band structure of germanium. In parentheses are the III-V compounds from which the pseudopotentials were extracted. All pseudopotentials given correspond to the lattice constant of pure Ge.

Pseudopotential	V_3	V_8	V_{11}
Ge[a]	−0.23	+0.01	+0.06
N(AlN,[b]GaN[b])	−0.36(1)	−0.178(2)	−0.10(1)
P(GaP,[a]AlP,[b]InP[a])	−0.33(2)	+0.002(2)	+0.05(1)
As(GaAs,[a]InAs[a])	−0.31(1)	−0.002(2)	+0.04(1)
Sb(GaSb,[a]InSb,[a]AlSb[a])	−0.30(1)	+0.03(1)	+0.052(7)
B(BN,[b]BP[b])	−0.27(1)	−0.08(2)	−0.02(2)
Al(AlSb,[a]AlP,[b]AlN[b])	−0.13(5)	+0.07(2)	+0.079(7)
Ga(GaP,[a]GaSb,[a]GaAs,[a]GaN[b]	−0.14(5)	+0.04(2)	+0.071(7)
In(InP,[a]InAs,[a]InSb[a])	−0.16(2)	+0.06(1)	+0.07(2)

[a]Reference 45.
[b]Reference 46.

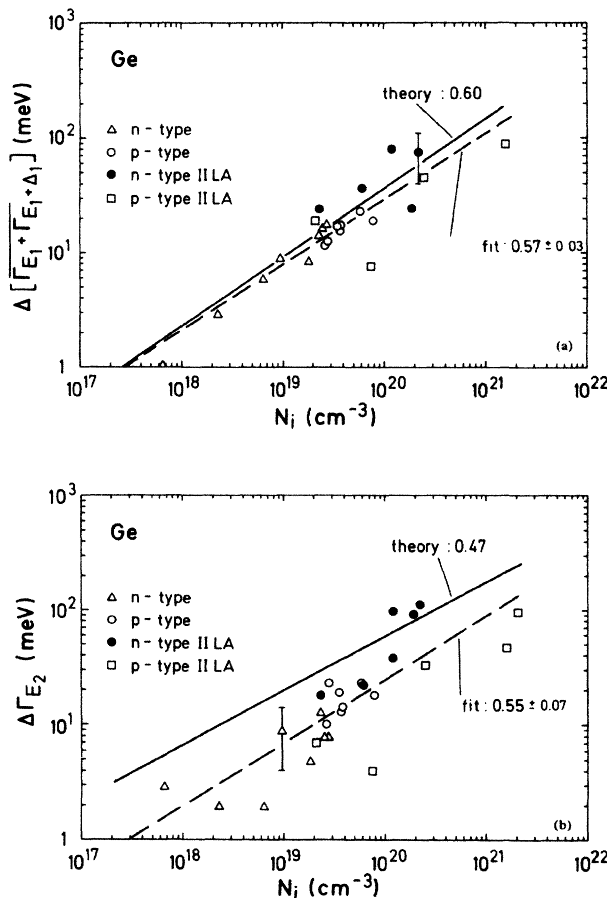

FIG. 5. Dependence on doping concentration of critical-point broadening parameters of Ge: (a) increase of the mean value of the broadening parameters Γ_{E_1} and $\Gamma_{E_1+\Delta_1}$ for the E_1 and $E_1+\Delta_1$ singularities; (b) increasing of the broadening parameter (Γ_{E_2}) for the E_2 singularity. The symbols have the same meaning as in Fig. 3. The best fit to a N_i^{α} law yields $\alpha=0.57\pm0.03$ for the E_1 transitions and $\alpha=0.55\pm0.07$ for E_2.

edges. Equations (15)–(18) of Ref. 23 are still valid for acceptors as well as for donors in Ge. The electrons in the conduction band in Si have **k** vectors in the [100] directions. The surface of constant energy are ellipsoids around the [100] directions in the parabolic-band approximation. The six valleys of Si are located in the vicinity of the $(2\pi/a_0)(0.85,0,0)$ point. The lowest conduction band of Ge is similar to that of Si, the main difference is the location of the valleys, which for Ge are four around the L points of the BZ. The transverse and longitudinal masses of electrons in Ge and Si are well known from cyclotron-resonance measurements. Their anisotropy is larger for Ge than for Si. We have listed in Table VI the effective masses of electrons and holes in Ge used in our calculations.

The second-order terms can be divided roughly into two categories. This division becomes clear when one considers the Thomas-Fermi (TF) approximation for the dielectric function. In this case Eqs. (16) and (17) of Ref. 23 take the form

$$\Delta^{(2)}_{\mathbf{k},n}(\Gamma_{\mathbf{k},n})\sim\frac{N}{(q^2+q_{\mathrm{TF}}^2)^2}\sim\frac{N}{(q^2+Cm_dN^{1/3})^2}\,, \quad (3)$$

where C is a constant $[C=(4\times3^{1/3})/\epsilon_0$, with ϵ_0 the q-independent static dielectric function of the undoped semiconductor], q_{TF}, the TF vector, and m_d the effective density-of-states mass:

$$m_{de}(\text{electrons})=n_v^{2/3}(m_Lm_T^2)^{1/3}\,, \quad (4a)$$

$$m_{dh}(\text{holes})=(m_l^{3/2}+m_h^{3/2})^{2/3}\,, \quad (4b)$$

with n_v the number of ellipsoids (four in the case of Ge). (The values of m_d are shown in Table VI.) According to Eq. (3) the perturbation diagrams for which q is large compared with $Cm_dN^{1/3}$ yield contributions to Δ proportional to N, while those for which q is small yield contributions proportional to $N^{1/3}$.

TABLE V. Linear coefficients dE_g/dN_i (in units of 10^{-24} eV cm^3) of the dependence of optical gaps on substitutional dopant concentration calculated by first-order perturbation theory in germanium. A positive $-dE_g/dN_i$ corresponds to a *red shift* upon doping. The limits of error correspond to calculations using pseudopotentials obtained for different III-V compounds. $E_{ind}(X)$ and $E_{ind}(L)$ represent the lowest gap at the X and L points, respectively.

				$-\frac{dE_g}{dN_i}$			
	E_0	E_0'	E_1	E_2	E_1'	$E_{ind}(X)$	$E_{ind}(L)$
N	204(16)	3(8)	94(10)	37(11)	4(9)	34(17)	89(12)
P	21(14)	−17(2)	−3(4)	−14(1)	−16(2)	−25(2)	−9(4)
As	26(3)	−10(1)	3(1)	−8(1)	−10(1)	−16(2)	−2(1)
Sb	3(3)	−10(2)	−9(1)	−14(1)	−10(2)	−21(2)	−12(1)
B	87(30)	4(5)	41(16)	19(8)	4(5)	19(9)	40(16)
Al	−53(6)	16(6)	−14(6)	4(10)	16(5)	15(12)	−8(10)
Ga	−32(7)	16(5)	−4(7)	9(6)	15(5)	20(10)	2(7)
In	−39(5)	13(4)	−10(2)	2(1)	13(4)	11(3)	−6(2)

Because of the many-valley character of the conduction band, m_d is larger for electrons than for holes, thus the screening should be more effective for electrons. From Eq. (3) one should therefore expect the effects of donors on the band structure of Ge to be less pronounced than for acceptors.

The TF approximation for the dielectric function overestimates, however, the screening for $q \geq q_{TF}$.[40] We have thus chosen the Lindhard approximation[41] for the q-dependent dielectric function:

$$\epsilon(q)=\epsilon_L(q)-\frac{4\pi}{q^2}\frac{1}{V}\sum_n F_n(q^*)\ , \qquad (5)$$

which describes the dielectric function in the random-phase approximation. In Eq. (5) V is the volume, $\epsilon_L(q)$ the dielectric function of the pure host semiconductor, and $F_n(q^*)$ is the Lindhard polarizability. The renormalized q, labeled q^*, is defined in Eqs. (6c) and (7c) for holes and electrons, respectively.

We have to distinguish in Eq. (5) between the case of acceptors and donors. The first case is the easiest one to

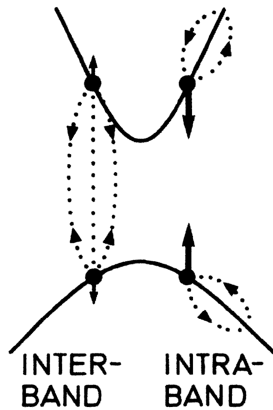

FIG. 6. Schematic representation of the shift of a band edge in second-order perturbation theory. Both inter- and intraband scattering are represented. The solid arrows show schematically the magnitude of both contributions and the sign of the shift produced by the interaction with an intermediate virtual state.

treat under the assumption of isotropic valence bands close to the Γ point. For holes, the index n in Eq. (5) takes the values l (for light holes) and h (for heavy holes). The following set of equations are valid for $k_BT \ll E_F$:

$$E_F=\frac{3\pi^2N_h^{2/3}}{2m_{dh}}\ , \qquad (6a)$$

$$[D(E_F)]_{l(h)}=\frac{(2m_{l(h)})^{3/2}}{2\pi^2}E_F^{1/2}\ , \qquad (6b)$$

$$q^*_{l(h)}=\frac{q}{(2E_Fm_{l(h)})^{1/2}}\ , \qquad (6c)$$

$$g(q)=\frac{1}{2}\left\{1-\frac{1}{q}\left[1-\left[\frac{q}{2}\right]^2\right]\ln\left[\frac{1-q/2}{1+q/2}\right]\right\}\ , \qquad (6d)$$

$$F_{l(h)}(q)=-V[D(E_F)]_{l(h)}g(q_{l(h)})\ , \qquad (6e)$$

where E_F is the Fermi energy and $[D(E_F)]_{l(h)}$ is the density of states at the Fermi energy. N_h is the hole density, whereby we assume all the impurities to be ionized.

In the case of donors one has to consider the anisotropy of the conduction band, and Eq. (6) has to be substituted by

$$E_F=\frac{3\pi^2N_e^{2/3}}{2m_{de}}\ , \qquad (7a)$$

$$[D(E_F)]=\frac{(2m_{de})^{3/2}}{2\pi^2n_v}E_F^{1/2}\ , \qquad (7b)$$

$$q_n^*=\frac{[\mu_{ij}^{(n)}q_iq_j]^{1/2}}{(2E_F)^{1/2}}\ , \qquad (7c)$$

where n stands for the n_v different valleys in Ge ($n_v=4$), N_e is the electron density, and $\mu_{ij}^{(n)}$ the inverse effective-mass tensor of the electrons in valley n, is defined as

$$e_n(\mathbf{k})=\mu_{ij}^{(n)}\mathbf{k}_i\mathbf{k}_j\ , \qquad (8)$$

where $e_n(\mathbf{k})$ is the unperturbed energy of an electron with wave vector $\mathbf{k}$ in band n. The other two equations (6d) and (6e) remain valid just changing the indices l and h by the index n of the n_v different valleys.

For the q-dependent dielectric function of the pure host

TABLE VI. Effective masses of electrons and holes of Ge in units of the free-electron mass. m_L and m_T are the longitudinal and transversal effective masses at the conduction-band minima $(2\pi/a)(0.5,0.5,0.5)$. lh and hh mean light and heavy holes, respectively. $m_{de(h)}$ is the effective density-of-states mass for electrons (holes).

	m_L	m_T	m_{lh}	m_{hh}	m_{de}	m_{dh}
Ge	1.58[a]	0.082[b]	0.042[b]	0.347[b]	0.55	0.36

[a]Reference 47.
[b]Reference 48.

semiconductor we have used Penn's interpolation formula,[42]

$$\epsilon_L(q)=1+\left[\frac{\omega_p^2}{E_g}\right]^2 D\left[1+\frac{E_F}{E_g}\left[\frac{q}{k_F}\right]^2 D^{1/2}\right]^{-2}, \quad (9)$$

where $D=1-\frac{1}{4}(E_g/E_F)$, $\omega_p^2=4\pi N_v$ (with N_v denoting the valence-electron concentration), $\mathbf{k}_F$ is the Fermi wave vector, and E_g a parameter representing an average energy gap (the Penn gap). In the case of Ge the following values were used: $\omega_p=15.6$ eV, $E_F=11.5$ eV, $\mathbf{k}_F=0.92$ bohr, and $E_g=4.2$ eV.

The rest of the equations of Sec. IV C of Ref. 23 remain the same and have been used to calculate the second-order terms of the effect of the impurities on the band structure of Ge.

A. E_0' gap

The E_0' CP of Ge corresponds to transitions between the $\Gamma_{25'}$ valence band and the Γ_{15} conduction band. This is the simplest for our calculations of self-energies because Eq. (28a) of VC has full cubic symmetry. The results are shown in Table VII for n- and p-type material and for two different concentrations. In Fig. 4(a) are shown the theoretical results (solid line) for p-doped Ge as a function of carrier concentration together with the experimental shifts and their best fit to an N_i^α law (dashed line). The theory represents well the experiments within their scatter. The exponent α is listed in Table VIII for the experimental as well as for the theoretical results.

B. E_1 gap

The E_1 and $E_1+\Delta_1$ CP are related to transitions along the Λ direction of the BZ between the Λ_6 and the Λ_{4-5} valence bands to the Λ_1 conduction band.[39] For a general point $\mathbf{k}$ along Λ, the $\mathbf{k}$ sum of Eq. (15) of VC is carried out over the irreducible part of the BZ. A sum is then performed over all vectors in the star of $\mathbf{k}$. Eight vectors of the star of $\mathbf{k}\{1,1,1\}$ were calculated and added to obtain the spectral function.

TABLE VII. Real part of the self energy and broadening of the E_0' and E_2 gaps of Ge calculated with second-order perturbation theory for two doping concentrations and both n- and p-type dopants. The point $(2\pi/a)(0.75,0.25,0.25)$ was chosen as representative of the E_2 transition.

N_i (cm^{-3})	$\Delta E_0'$ (meV)	ΔE_2 (meV)	$\Delta\Gamma_{E_2}$ (meV)
	n type		
5×10^{18}	3	2	4
5×10^{20}	50	40	90
	p type		
5×10^{18}	6	3	14
5×10^{20}	60	50	110

The calculated Lorentzian-broadening parameters of the valence and conduction bands (VB and CB, respectively) together with the total broadening along the Λ direction are shown in Fig. 7 for electrons and holes in Ge with a carrier concentration of 5×10^{20} cm^{-3}. The differences between the band edges of Si and Ge are responsible for the fact that in Ge the total broadening at the Γ point is smaller than in Si (see Fig. 8 of Ref. 23) (the DOS at $\Gamma_{2'}$ CB of Ge is much smaller than that of Si at the Γ_{15} CB). The results for p-type material are qualitatively the same, although somewhat larger than for their n-type counterparts. This fact confirms our argument, based on the TF approximation, of a more effective screening by electrons than by holes. The major contribution to the broadening is seen to arise, as in the case of Si, from the conduction-band states and from $\mathbf{k}$ points close to $[(\pi/4a)](1,1,1)$. For $\mathbf{k}<[(\pi/2a)](1,1,1)$ the major contribution arises from the valence-band states. In Fig. 8 the shifts are shown also for p- and n-type Ge with a carrier concentration of 5×10^{20} cm^{-3}. The total red shifts arise from a down shift of the conduction band and up shift of the valence band. The contributions of each of both bands are of the same order over a large region of the Γ-L points. Again, as in the case of the broadenings, the shifts are slightly larger in the case of p-doped Ge.

The directly measurable quantities, the total shifts, and the increases of Lorentzian broadenings, for the E_1 singularity, are taken to be the average of those from

TABLE VIII. Values of α obtained from the fits of the shifts and broadenings of the different band gaps of Ge with doping concentration N_i to a N_i^α law. Experimental data for n- and p-type Ge were fitted simultaneously. The calculated shifts were fitted separately in the n- and the p-type case.

	E_1	E_0'	E_2	$\Gamma(E_1)$	$\Gamma(E_2)$
			Expt.		
	0.63(4)	0.45(3)	0.61(5)	0.57(3)	0.55(7)
			Calc.		
n-type	0.61	0.45	0.57	0.61	0.46
p-type	0.64	0.46	0.61	0.60	0.47

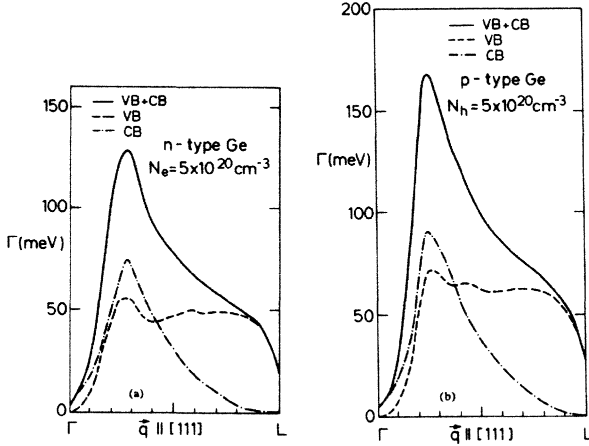

FIG. 7. Lorentzian-broadening parameter along the Λ direction in Ge with a carrier concentration of $N = 5\times10^{20}$ cm^{-3} (a) n-type Ge, (b) p-type Ge. Dotted-dashed lines: broadening of states at the lowest conduction band (Γ_{CB}). Dashed lines: broadening of states at the highest valence band (Γ_{VB}). Solid line: total broadening parameter ($\Gamma = \Gamma_{VB} + \Gamma_{CB}$).

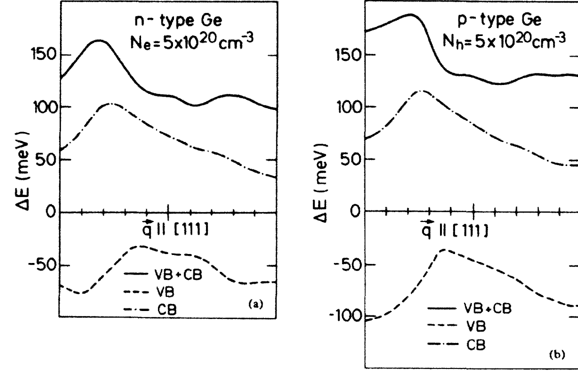

FIG. 8. Energy shifts obtained by second-order perturbation theory for germanium with a carrier concentration $N = 5\times10^{20}$ along the Λ direction of the Brillouin zone. (a) n-type Ge, (b) p-type Ge. Dotted-dashed line: real part of the self-energy for states at the lowest conduction band (CB). Dashed line: real part of the self energy for states at the highest valence band (VB). Solid line: total second-order red shift of the band gap (VB + CB).

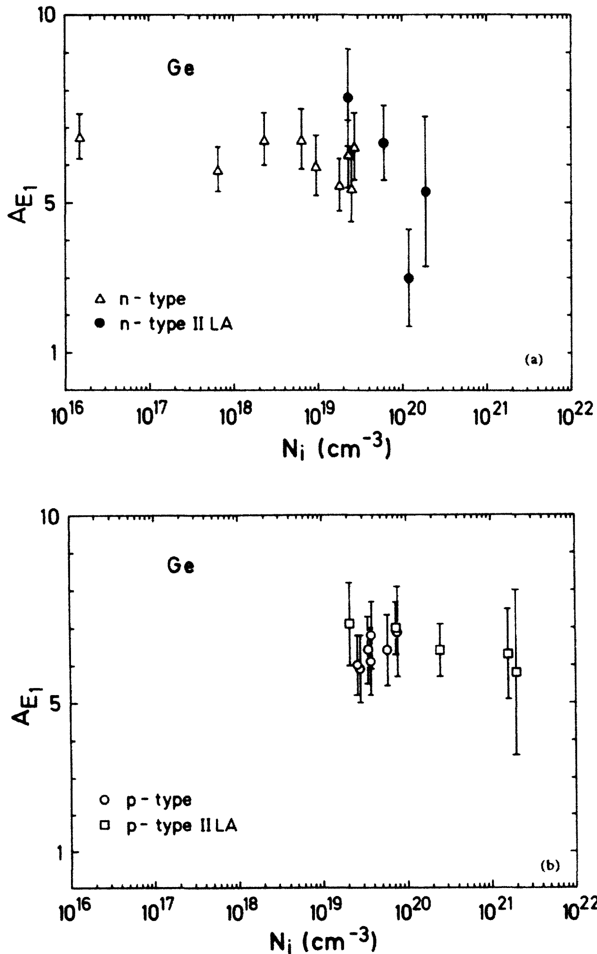

FIG. 9. Amplitudes of the E_1 singularity of doped germanium. (a) n-type Ge, (b) p-type Ge. The symbols have the same meaning as in Fig. 3.

$\mathbf{k} = [(\pi/4a)](1,1,1)$ to the L point [a mesh $0.02(2\pi/a)$ was used]. The calculated averages for p doping are shown by a solid line in Figs. 4(b) and 5(a) for the shifts and broadenings, respectively, as a function of carrier concentration together with the experimental points and the best fit (dashed lines) to a N_i^α law. The theoretical results for n doping are slightly smaller than those of p doping. In Table VIII the exponents α are also listed. The agreement between theory and experiment is satisfactory.

C. E_2 gap

For the E_2 CP we have made calculations at the point $[(2\pi/a)](0.75,0.25,0.25)$ (Ref. 39). In this case the star of $\mathbf{k}$ contains 24 points. The results for two different concentrations are listed in Table VII. In Figs. 4(c) and 5(b) are shown the theoretical results for the shifts and the broadenings, respectively, together with experimental points and the best fit with N_i^α. The agreement between theory and experiment is here reasonably good.

V. DISCUSSION

The previously observed blurring of the E_1 peak in Si has been also found in our present measurements on Ge. Assuming that the excitonic interaction is screened by the free carriers and in the contact-interaction approximation, we have fitted $\tan\phi$ with Eq. (30) of Ref. 23. We have used an average effective mass m_d of 0.47 for Ge and obtained an excitonic radius $r_{exc} = (9\pm1)$ Å, the same value as in the case of Si (Ref. 23) and in very good agreement with the value found for the E_1 exciton of GaAs (10 Å).[43]

The dependence on the impurity concentration of the amplitudes of the E_1 transitions for n and p doping is shown in Figs. 9(a) and 9(b). Within the experimental uncertainty A_{E_1} for p doping shows no dependence on im-

purity concentration; however, an indication of a decrease of A_{E_1} is present for n-type Ge. A possible explanation of this fact could be the filling of the L conduction-band minima, with increasing impurity concentration. This fact has also been observed recently in resonant Raman scattering[20] and attributed to blocking of the interband transitions caused by carriers at the L point in the CB; however, effects due to poor annealing of the samples cannot be discarded as a possible cause of this decrease.[20]

We have fitted the shifts and broadenings of Figs. 4 and 5 with the function CN_I^{α} (C equals constant) and find values of α close to 0.5. The first-order perturbation shifts given in Table V are negligible except for $N_i > 10^{21}$ cm^{-3}. We find no experimental evidence for these linear shifts and therefore neglect them. The predictions of the second-order perturbation calculation are in good agreement with the experimental results.

In our calculations, many-body effects have been neglected. These effects, where exchange as well as correlation play a dominant role, are responsible for the shrinkage of the lowest band edges, and have been profusely studied in the literature.[49–52] In the case of the higher edges studied in the present work, the exchange plays only a small role, due to the fact that the carriers are located in a region of **k** different from the region where the electronic interband transitions take place. On the other hand, correlation terms, which are known to dominate the fundamental band-gap shrinkage,[51] could give important contributions to the shifts of the higher band edges.

Finally, we would like to mention that the first-order contribution, found to be small in our calculations, will be partly canceled by a corresponding electron-electron interaction term. This term, arising from the electrostatic energy between the charge density of a particle and that of the dopant carriers, would, in the long-wavelength limit, exactly cancel the first-order impurity contribution.

VI. SUMMARY

We have measured the effect of heavy doping, both n and p type, on the interband transitions of Ge. Concordant results have been found for bulk and IILA samples. Complete pseudopotential band-structure calculations of the self-energies of the critical points agree with the experimental results. A noticeable decrease of the excitonic effects on the E_1 singularity has been quantitatively studied: it is believed to be due to the screening of the excitonic interaction by the free carriers. A blocking of the E_1 interband transitions, attributed to increasing filling of the L minima of the conduction band in the case of n-doped material has also been observed.

ACKNOWLEDGMENTS

We would like to thank G. Kisela and A. Breitschwert for sample preparation and characterization, and H. Bleder and A. Birkner for help with construction of the ellipsometer. We also thank Dr. A. Axmann for the ion implantation of the IILA samples and P. B. Allen for providing computer programs.

*Present address: IBM Thomas J. Watson Research Center, Yorktown Heights, P.O. Box 218, NY 10598. Permanent address: Instituto de Ciencia de Materiales del Consejo Superior de Investigaciones Científicas, Universidad de Zaragoza E-50009 Zaragoza, Spain.

[1]R. A. Abram, G. J. Rees, and B. L. H. Wilson, Adv. Phys. **27**, 799 (1978).

[2]R. W. Keyes, Comments Solid State Phys. **7**, 149 (1977).

[3]H. Fritzsche, in *The Metal Non-Metal transition in Disordered Systems,* edited by L. R. Friedman and D. P. Tunstall (Scottish Universities Summer School Program, Edinburgh, 1978).

[4]J. W. Slotboom and H. C. de Graaf, Solid-State Electron. **19**, 857 (1976).

[5]J. I. Pankove, Phys. Rev. Lett. **4**, 454 (1960); J. I. Pankove and P. Aigrain, Phys. Rev. **126**, 956 (1962).

[6]C. Haas, Phys. Rev. **125**, 1965 (1962).

[7]F. Lukeš and J. Humlíček, Phys. Rev. B **6**, 521 (1972).

[8]J. Wagner and L. Viña, Phys. Rev. B **30**, 7030 (1984), and references therein.

[9]E. Burstein, Phys. Rev. **93**, 632 (1954).

[10]M. Cardona and H. Sommers, Jr., Phys. Rev. **122**, 1382 (1961).

[11]M. Cardona and W. Paul, Helv. Phys. Acta **33**, 329 (1960).

[12]G. B. Dubrovskii and V. K. Subashiev, Fiz. Tverd. Tela (Leningrad) **5**, 1104 (1963) [Sov. Phys.—Solid State **5**, 805 (1963)].

[13]F. Lukeš and E. Schmidt, in *Proceedings of the 7th International Conference on the Physics of Semiconductors, Paris, 1964,* edited by M. Hulin (Dunod, Paris, 1964), p. 197.

[14]M. Cardona, K. L. Shaklee, and F. H. Pollak, Phys. Rev. **154**, 696 (1967).

[15]J. Humlíček, Phys. Status Solidi B **86**, 303 (1978).

[16]F. Lukeš, E. Schmidt, and H. Humlíček, in *Proceedings of the 11th International Conference on the Physics of Semiconductors, Warsaw, 1972* (Polish Scientific Publishers, Warsaw, 1972), p. 1382.

[17]J. Humlíček and F. Lukeš, Phys. Status Solidi **71**, 315 (1975).

[18]G. Contreras, A. Compaan, J. Wagner, M. Cardona, and A. Axmann, J. Phys. (Paris) Colloq. **44**, C5-55 (1983).

[19]L. Viña and M. Cardona, Physica **117& 118B**, 356 (1983).

[20]A. K. Sood, G. Contreras, and M. Cardona, Phys. Rev. B **31**, 3760 (1985).

[21]D. E. Aspnes, G. K. Celler, J. M. Poate, G. A. Rozgonyi, and T. T. Sheng in *Laser and Electron Beam Processing of Electronic Materials,* edited by C. L. Anderson, G. K. Celler, and G. A. Rozgonyi (Electrochemical Society, Princeton, New Jersey, 1980), p. 414; D. E. Aspnes, A. A. Studna, and E. Kinsbron, Phys. Rev. B **29**, 768 (1984).

[22]G. E. Jellison, Jr., F. A. Modine, C. W. White, R. F. Wood, and R. T. Young, Phys. Rev. Lett. **46**, 1414 (1981).

[23]L. Viña and M. Cardona, Phys. Rev. B **29**, 6739 (1984).

[24]A. Compaan, G. Contreras, M. Cardona, and A. Axmann, in *Proceedings of Material Research Society,* edited by J. C. Fan and N. M. Johnson (North-Holland, New York, 1984), Vol. 23, p. 117, and references therein.

[25]P. B. Allen, Phys. Rev. B **18**, 5217 (1978); B. Chakraborty and P. B. Allen, *ibid.* **18**, 5225 (1978).

[26]The crystals were implanted by Dr. A. Axmann at the Frauenhofer-Institut für angewandte Festkörpephysik, Freiburg, Federal Republic of Germany.

[27]A. Compaan, G. Contreras, M. Cardona, and A. Axmann, in

Proceedings of the Material Research Society, Symposium on Laser Processing of Materials, Strasbourg, 1983, [J. Phys. (Paris) Colloq. **44**, C5-193 (1983)].

[28]D. E. Aspnes, J. Opt. Soc. Am. **64**, 812 (1974).

[29]N. M. Bashara and R. M. Azzam in *Ellipsometry and Polarized Light* (North-Holland, Amsterdam, 1977).

[30]Another possibility is that the implanted film did not recrystalize completely after the laser annealing. As a consequence of this top layer would be damaged, as recently shown in the case of Si [A. Borghesi, Chen Chen-Jia, G. Guizzetti, L. Nosenzo, A. Stella, S. U. Campisano, and E. Rimini, J. Appl. Phys. **58**, 2773 (1985)]. The differences between a damaged layer and an oxide layer could not be resolved in our measurements.

[31]G. G. Devyatykh, E. M. Dianov, N. S. Karpychev, S. M. Mazavin, V. M. Mashinskii, V. B. Neustruev, A. V. Nikolaichick, A. M. Prokhorov, A. I. Ritus, N. I. Sokolov, and A. S. Yushing, Sov. J. Quantum Electron. **10**, 900 (1981).

[32]A. S. Householder, *Principles of Numerical Analysis* (McGraw-Hill, New York, 1953).

[33]D. L. Greenaway and G. Harbeke, *Optical Properties and Band Structure of Semiconductors* (Pergamon, London, 1968).

[34]H. R. Philipp and H. Ehrenreich, Phys. Rev. **129**, 1550 (1963).

[35]M. Cardona, *Solid State Physics,* edited by F. Seitz, D. Turnbull, and H. Ehrenreich (Academic, New York, 1969), Suppl. 11.

[36]L. Viña, S. Logothetidis, and M. Cardona, Phys. Rev. B **30**, 1979 (1984).

[37]Y. Toyozawa, M. Inoue, Y. Inui, M. Okazaki, and E. Hanamura, J. Phys. Soc. Jpn. Suppl. **21**, 133 (1967); J. E. Rowe and D. E. Aspnes, Phys. Rev. Lett. **25**, 162 (1970).

[38]C. W. White, P. P. Pronki, S. R. Wilson, B. R. Appleton, J. Narayan, and R. T. Young, J. Appl. Phys. **50**, 3261 (1979).

[39]J. R. Chelikowsky and M. L. Cohen, Phys. Rev. B **14**, 556 (1976).

[40]C. Haas, Phys. Rev. **125**, 1965 (1962).

[41]J. Lindhard, K. Dan. Vidensk. Selsk. Mat.-Fys. Medd. **28**, No. 8 (1954).

[42]D. R. Penn, Phys. Rev. **128**, 2093 (1962).

[43]J. E. Rowe, F. H. Pollak, and M. Cardona, Phys. Rev. Lett. **22**, 933 (1969).

[44]G. Contreras, L. Tapfer, A. K. Sood, and M. Cardona, Phys. Status Solidi B **131**, 457 (1985).

[45]M. L. Cohen and T. K. Bergstresser, Phys. Rev. **141**, 789 (1966).

[46]J. A. Sanjurjo, E. López-Cruz, P. Vogl, and M. Cardona, Phys. Rev. B **28**, 4579 (1983).

[47]W. C. Dash and R. Newmann, Phys. Rev. B **99**, 1151 (1955).

[48]J. C. Hensel and K. Suzuki, Phys. Rev. B **9**, 4219 (1974).

[49]J. C. Inkson, J. Phys. C **9**, 1170 (1970).

[50]G. D. Mahan, J. Appl. Phys. **51**, 2634 (1980).

[51]K.-F. Berggren and B. E. Sernelius, Phys. Rev. B **24**, 1971 (1981).

[52]A. Selloni and T. Pantelides, Phys. Rev. Lett. **49**, 586 (1982).